Journal of Laser Applications

RESEARCH ARTICLE | SEPTEMBER 17 2024

Study of burst mode for enhancing the ps-laser cutting performance of lithium-ion battery electrodes

Special Collection: Laser Manufacturing for Future Mobility

Pourya Heidari Orojloo ; Ali Gökhan Demir

J. Laser Appl. 36, 042013 (2024)
https://doi.org/10.2351/7.0001417

Journal of Laser Applications ARTICLE pubs.aip.org/lia/jla

Study of burst mode for enhancing the ps-laser cutting performance of lithium-ion battery electrodes

Cite as: J. Laser Appl. 36, 042013 (2024); doi: 10.2351/7.0001417
Submitted: 1 May 2024 · Accepted: 19 August 2024 ·
Published Online: 17 September 2024

Pourya Heidari Orojloo[a] and Ali Gökhan Demir

AFFILIATIONS

Department of Mechanical Engineering, Politecnico di Milano, Via La Masa 1, 20156 Milan, Italy

Note: Paper published as part of the special topic on Laser Manufacturing for Future Mobility
[a]**Author to whom correspondence should be addressed, electronic mail:** pourya.heidari@polimi.it

ABSTRACT

The demand for lithium-ion batteries (LIBs) has increased significantly, leading to an increased focus on high quality production methods. In response to this growing demand, laser technology has been increasingly used for electrode notching and cutting. In addition, the advent of high-power ultrashort lasers equipped with burst mode capabilities represents a promising option for electrode cutting of LIBs. On the other hand, these types of lasers for this purpose are relatively unexplored in the literature. This study investigates the effect of various parameters, including the number of pulses per burst (ranging from 1 to 8), the pulse repetition rate (200.0, 550.3, and 901.0 kHz), and the burst shape (equal pulse peak and increasing pulse peak), on the laser cutting process of aluminum foil, cathode, copper foil, and anode. The results indicate that increasing the number of pulses per burst and the pulse repetition rate improves productivity and quality for all materials, with a more significant effect observed for metal foil than for cathode and anode materials due to the different laser-material interactions for metal foil and active material. The burst shape with equal pulse peaks was found to be a more suitable temporal distribution for cutting all materials compared to an increasing pulse peak distribution. The ablation efficiency was evaluated as a function of the peak fluence of a single pulse within the burst. The results emphasize that higher productivity at higher average power can be achieved by increasing the pulse repetition rate toward the MHz range with moderate pulse energies.

Key words: remote laser cutting, lithium-ion battery electrodes, burst mode, ps-pulsed laser system, laser micromachining, ultrashort pulsed lasers

I. INTRODUCTION

With current technological advances in cleaner energy and more efficient battery production methods, lithium-based battery electric vehicles (EVs) appear to offer a promising way forward.[1] Recent forecasts predict a remarkable increase in global demand for lithium-ion batteries (LIBs) over the next decade. Estimated demand is expected to increase from around 0.7 TWh in 2022 to around 4.7 TWh in 2030. The vast majority of this demand in 2030, around 4.3 TWh, will come from batteries used in mobility applications, particularly EVs, due to the rapid growth of the mobility sector.[2] The manufacturing process of LIBs consists of three main stages: electrode preparation, cell assembly, and activation of the battery electrochemistry. Defects occurring in the early stages of the production line can lead to increased costs and material waste.[3]

To meet the growing demands of LIB manufacturing, it is essential to use the appropriate tools. Laser technology is a practical option, serving as a versatile digital tool that, unlike conventional methods, offers scalability, precision, and flexibility across different manufacturing stages. Laser drying of active material,[4] laser notching of metal foils,[5,6] cutting of electrodes,[7–11] laser welding of tabs and enclosure,[12–15] laser structuring of active material,[16–18] and laser welding of busbar to pack cell[19–21] represent various applications of lasers as tools in LIB manufacturing. In electrode preparation, several factors can influence the thickness and density of the

electrode, all of which have the potential to affect laser cutting processes. It is noteworthy that the increasing use of lithium metal foil as an anode in solid-state batteries requires precise cutting, highlighting the usefulness of lasers as cutting tools, especially considering that lithium metal is adhesive, posing a challenge to conventional mechanical cutting methods.[22–25]

There are numerous combinations of laser systems suitable for electrode notching and cutting, requiring considerable effort to select the appropriate laser system for electrode cutting. Regarding the quality of the cut metal foil, a small portion of the molten material solidifies at the edge during the laser-material interaction, forming a so-called burr. During the laser cutting of the anode and cathode, in addition to separating the electrodes, a small portion of the coating is removed exposing the metallic layer. This phenomenon, defined as clearance, predisposes the electrodes to short circuits during LIB cycling if it exceeds a certain threshold. Demir and Previtali[26] investigated the quality aspects of laser cutting for LIB electrodes, comparing the use of a nanosecond pulsed (ns-pulsed) laser source with the green and near-infrared wavelengths. Lutey *et al.*[27] investigated the laser cutting of lithium iron phosphate electrodes using both continuous wave (CW) and ns-pulsed laser systems with different laser specifications such as wavelength and pulse duration. Lee and Anh[28] conducted a study on the surface morphology of cathodes cut by a CW laser system, focusing on the definition of significant cutting widths such as top width, melting width, and kerf width to investigate the physical phenomena involved in laser material removal. Kriegler *et al.*[29] compared ns-pulsed, picosecond pulsed (ps-pulsed), and CW laser systems for their potential for electrode cutting in LIB production. The CW laser system achieved cutting speeds of up to 10 m/s, exceeding the productivity achievable with pulsed laser sources. Therefore, ps-pulsed laser systems with higher pulse repetition rates (PRRs), combined with high-speed galvanometer or polygon scanners, are considered promising alternatives to establish ns-pulsed laser systems.

In addition to the experimental approach, there have been several publications by Lee *et al.* on the simulation of laser cutting of anodes,[30] cathodes,[31] and current collectors.[32] These simulations have been validated using a near-infrared CW laser. These studies improve our understanding of the cutting mechanisms during laser processing of electrodes. The simulations show that laser cutting of copper (Cu) current collector depends on both laser intensity and interaction time, while aluminum (Al) current collector cutting is more dependent on laser intensity. In contrast, simulations of anodes and cathodes show that penetration depth and absorptivity change significantly when the deep penetration hole reaches the material interface. This is mainly due to melt pool flow patterns, temperature distribution, material properties, and composition changes at the interface.

In metal micromachining with ultrashort pulse laser systems, it is critical to adjust the peak fluence to an optimum level as this helps to increase the material removal per pulse energy.[33] Setting the optimum peak fluence ensures that the laser energy is effectively used for material removal rather than being dissipated into the material as heat increases the temperature. Recently, laser source suppliers have developed high-power ultrashort laser systems with innovative features such as burst mode. This functionality provides an additional level of control to adjust the energy per pulse. Neuenschwander *et al.*[34] showed that the reduction of the energy in a single pulse within the burst is the primary factor contributing to the often-reported increase in removal rate when using burst mode. In the case of Cu, burst mode resulted in a genuine increase in the removal rate of approximately 20%.

The ultrashort laser system equipped with burst mode capability can be used to optimize the laser notching and cutting of electrodes in the production line of LIBs. Haung *et al.*[35] conducted a study on the effects of burst mode on laser cutting productivity and quality of anode and Cu foil. The bursts consisted of ps pulses with short interval delays in the ns range. The effects of 2–10 pulses in a burst on the kerf edges were analyzed and compared with those of a single pulse. The study of anode edge shapes under different conditions showed that the burst mode resulted in a smaller heat affected zone (HAZ) of the Cu current collector and a narrower clearance width of the graphite anode material. The results showed a significant increase in cutting efficiency as the number of pulses in a burst increased, with maximum cutting speeds for the Cu current collector and graphite anode material reaching 3.8 and 0.5 m/s, respectively. While the availability of power and pulse repetition rates of ps-pulsed lasers is increasing, systematic studies of the different anode and cathode materials using burst mode appear to be missing in the literature. To the authors' knowledge, no previous work has provided an in-depth analysis of the pulse peak power, energy, and their effects on cutting productivity for conventional anodes, Cu foil, cathodes, and Al foils used in LIBs.

Accordingly, this work investigates how different factors, such as the number of pulses per burst, pulse repetition rate, and burst shape, affect the laser cutting of Al foil, cathode, Cu foil, and anode. The process parameters were studied to investigate the process feasibility windows highlighting the maximum cutting speed per burst profile. The results were analyzed in terms of kerf quality and showed the ideal pulse train conditions for each material. Analytical modeling was used as an aid to estimate the laser source characteristics for scaling up the productivity of the process.

II. PULSE AND BURST ENERGY CONTROL

Pulsed wave (PW) lasers operate with several parameters that control the temporal pulse profile. Pulse duration (τ) is a characterizing parameter in laser-material interaction, and laser sources are typically classified into long (ms-μs), short (ns), and ultrashort (ps-fs) pulsed categories based on this factor. While the pulse duration is typically fixed for most laser sources, changing it can affect the laser-material interaction. In long-pulsed systems, the interaction is primarily melting based, whereas in ultrashort pulsed laser systems, it is ablation based.[36] Burst mode is commonly available for ultrafast laser sources and refers to multiple consecutive pulses released at the same PRR with a given intraburst delay, allowing the energy to be split into a faster pulse train. Essentially, burst mode reduces the energy and the peak power of a single pulse into small and fast bursts. Conventionally, the pulse repetition rate of ultrafast laser sources is in the kHz to MHz range, while the delays can vary from tens of ns to hundreds of ps.

Figure 1 illustrates the differences between the conventional pulsation and burst mode. As shown in Fig. 1(a), in conventional

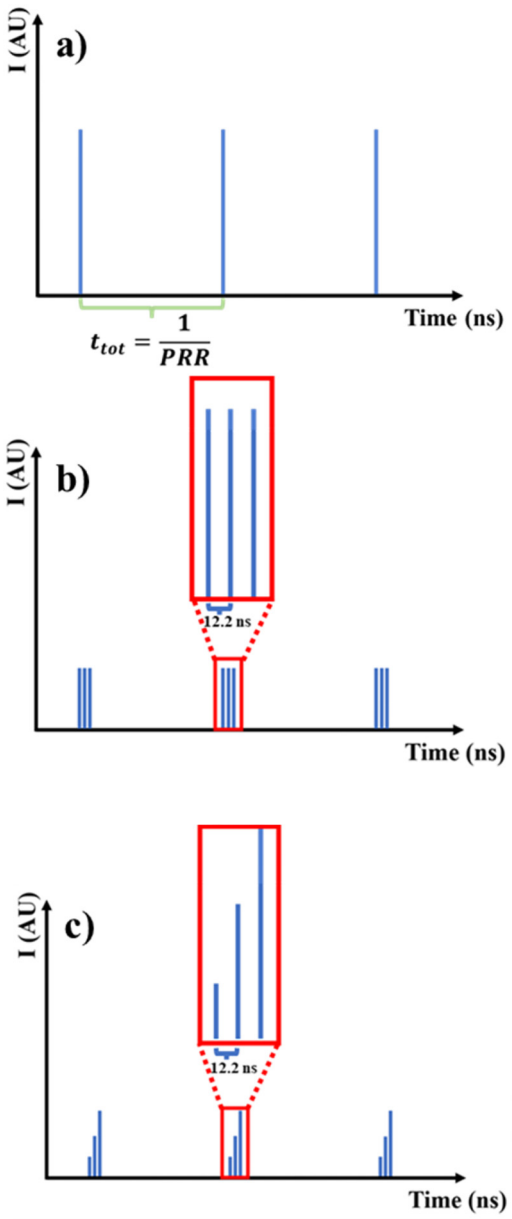

FIG. 1. Temporal distribution of ps-pulsed laser system (a) without the burst mode, (b) equal peak of the pulses in a burst, and (c) increasing trend of the pulses peak in a burst.

pulsed wave mode, the pulses are sent at a fixed PRR. In burst mode, the burst packages are sent at the same time interval, while the bursts are sent with the intraburst delay as shown in Fig. 1(b). The profile of the burst train can be adjusted to test different interaction mechanisms, for example, using an increasing profile as shown in Fig. 1(c).[34]

For conventional pulsed wave emission without burst mode, the energy within each pulse can be calculated as follows:

$$E = \frac{P_{\text{avg}}}{PRR}, \tag{1}$$

where E is the energy of each pulse and P_{avg} is the average power of the laser source. In the burst mode, the energy of each pulse within the burst is modified as follows:

$$E = \frac{P_{\text{avg}}}{PRR \cdot Nb}, \tag{2}$$

where Nb is the number of pulses in the burst. The peak power of each pulse is equal to

$$P_{pk} = \frac{E}{\tau}, \tag{3}$$

where P_{pk} is the peak power of a single pulse. Note that P_{pk} is calculated using a square wave approximation. One way of estimating the cutting capability of given parameter combinations is to use a lumped heat capacity model. The model uses an energy balance to melt the given amount of material and has also been used for ns-pulsed laser cutting of electrodes.[26] The model establishes a simple relationship between the power to thickness ratio and the maximum cutting speed. For a pulsed emission wave with a fixed average power, the use of the peak power can be considered to assess whether the following expression applies

$$v_c \propto \frac{P_{\text{avg}}}{t} \propto \frac{P_{pk}}{t}, \tag{4}$$

where v_c is the maximum cutting speed and t is the electrode thickness. The model can also be used to evaluate the differences in processability between different bare and electrode materials, taking into account their thicknesses.

On the other hand, the process of removing metal foil with the ultrashort laser can clarify why the efficiency of laser cutting of metal foil is increasing. Fluence is a critical parameter in determining the energy per irradiated area. Peak fluence is equal to

$$\phi_0 = \frac{8 \cdot E}{\pi \cdot d_0^2}, \tag{5}$$

where d_0 is the spot diameter at the focal point and ϕ_0 is the peak fluence of each pulse. One quantity used to describe an ablation efficiency is the energy specific volume, which is the volume of material per pulse energy for a single pulse. For the Gaussian laser beam, the energy specific volume is equal to[34]

$$ESV = \frac{V}{E} = \frac{1}{2} \cdot \frac{\delta}{\phi_0} \cdot \ln^2\left(\frac{\phi_0}{\phi_{th}}\right), \tag{6}$$

where δ is the effective penetration depth of the pulse energy, ϕ_{th} is the ablation threshold, and ESV is the energy specific volume. In the case of single pulse ablation, the model has been shown to provide the optimum ablation conditions in terms of material

removal efficiency when the following conditions are satisfied:

$$\phi_{0,opt} = e^2 \phi_{th}, \tag{7}$$

where $\phi_{0,opt}$ is the optimum peak fluence for the material removal. The existence of an optimum peak fluence level has been shown for various materials in the literature. In the case of a multilayer material such as the electrodes, the existence of a single ablation threshold is not reasonable. On the other hand, the ideal condition for the maximum material removal efficiency may exist and can be demonstrated experimentally. Therefore, in the case of electrode cutting with burst mode, the volume removed by a single pulse can be calculated directly using the following formula:

$$V = \frac{t \cdot w_k \cdot v_c}{PRR \cdot Nb}, \tag{8}$$

where w_k is the kerf width and V is the volume removed by a single pulse. It should be noted that the energy specific volume has been effectively used in bulk ablation studies. However, its use in laser cutting applications neglects the energy loss due to the open kerf. In the case of the anode and cathode, composite layered materials, the kerf width is not constant as the material changes along the thickness due to clearance formation. The model can provide a valid approximation to identify the optimum peak fluence for the most efficient material removal through cutting experiments. For complete cuts where the cutting speed, pulse repetition rate, and number of pulses per burst are known, the kerf width can be measured. From this, the volume per pulse and volume per pulse energy can be calculated. The model can be fitted to the experimental data to estimate the threshold fluence and effective penetration depth, and hence also the optimum peak fluence. Upscaling of the cutting process can be achieved by increasing the laser power through increasing the pulse repetition rate at the optimum pulse energy. The pulse repetition rate required to achieve the desired cutting speed can be calculated by substituting the volume removed by a single pulse [Eq. (8)], the energy of the pulse [Eq. (5)], and the optimum value of the peak fluence [Eq. (7)] into the ablation efficiency model [Eq. (6)],

$$PRR = \frac{4 \cdot t \cdot w_k \cdot v_c}{\delta \cdot \pi \cdot d_0^2}. \tag{9}$$

According to the formulation, when the optimum peak fluence is used, the kerf width is equal to the beam diameter ($w_k = d_0$).

The model in its current form neglects material variations in the thickness, making it difficult to apply to anode and cathode materials. Another point concerns the intrinsic variation of the pulse repetition rate when considering the single pulse energy within the burst. In the literature, the optimum ablation conditions are sought separately for different pulse durations, pulse repetition rates, and pulse numbers within a burst.[24,37–40] While such simplifications limit the applicability of the model to the electrode cutting, it can be used as a descriptive tool to understand the influence of the energy content of a single pulse within the burst.

The validity of the two proposed models based on peak power and optimum peak fluence was sought through a comprehensive experimental analysis.

III. MATERIALS AND METHODS

A. Electrodes

The basic components of LIBs are the anode, cathode, and separator. Both the cathode and anode consist of three layers, with two active layers sandwiching a metallic layer that acts as an electron collector. The active material typically consists of porous particles bound together by a binder. The operation of LIBs is based on the intercalation of lithium ions between the active materials of the anodes and cathodes. The active materials of the anode electrode are 94% Gr (graphite) + 2% C65 (carbon black) + 2% CMC (carboxymethyl cellulose) + 2% SBR (styrene-butadiene rubber) with a thickness of 50 μm on each side. Conversely, the active material of the cathode is lithium metal oxide [95% NMC622 (nickel manganese cobalt) + 3% C65 (carbon black)+ 3% PVDF (polyvinylidene fluoride)] with a thickness of 30 μm. The electron collectors are made of Cu and Al foils, with thicknesses of 11 and 13 μm, respectively. Figure 2 shows a graphical representation of the cathode, anode, Al, and Cu foils and their respective thicknesses.

B. Laser cutting system

The laser system operates in the ps regime and uses a near-infrared wavelength of 1064 nm to cut the cathode, anode, Al foil, and Cu foil. This laser source has a pulse duration of 10 ps and a maximum average power of 50 W (Lumentum Picoblade 2). It offers a wide range of pulse repetition rates and has burst mode capability with an intraburst delay of 12.2 ns. The laser source can operate at discrete levels of pulse repetition rates between 200 and 8200 kHz. The collimated beam exiting the laser source has been expanded to 15 mm before entering the scanner head. A galvanometric scanner head (Raylase Miniscan III-20) steers the beam and an f-theta lens (Qioptiq 4401-288-000-20) with a focal length of

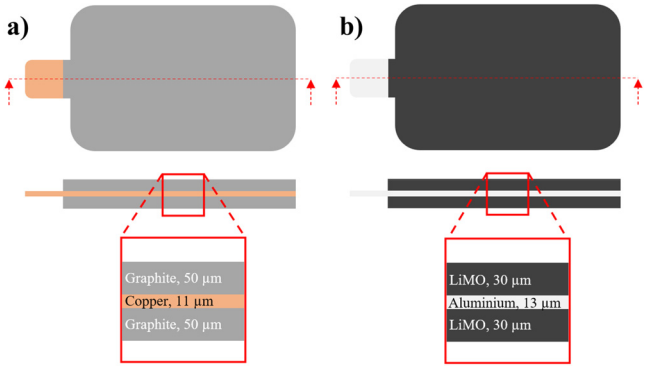

FIG. 2. Graphical representation of (a) anode and (b) cathode.

TABLE I. General specifications of the used laser system.

Parameter	Value
Wavelength, λ (nm)	1064
Max. average power, P_{avg} (W)	50
Pulse repetition rate, PRR (kHz)	200–8200
Pulse duration, τ (ps)	10
Beam quality, M^2	1.2
Polarization state	Linear
Collimated beam diameter, d_c (mm)	15
Focal length, f_f (mm)	254
Calculated diameter at focal point, d_0 (μm)	27.5

254 mm focuses it to a point with a focal diameter of 27.5 μm. The burst profile can be varied by setting gain factors for each pulse for up to eight pulses within the burst. The gain factors have been modified to provide flat and increasing burst profiles. Table I reports the general specifications of the laser system. The experimental procedure was carried out in a normal environment without humidity control, with careful handling of the material. Figure 3 describes the integrated systems used for the experiments.

C. Characterization

To characterize the burst shape, a fast photodiode was used to acquire the power profile. The laser beam was directed onto the photodiode (Thorlabs DET10A2), which converts light energy into electrical current with a rise time of 1 ns. The photodiode was able to capture the shape of the pulse train but was unable to resolve the shape of the single pulse. A digital oscilloscope (MSO 4024, RIGOL) was used to record the signals.

In addition, the quality characteristics of the cuts were assessed using scanning electron microscope (SEM) images (Zeiss EVO 50). These images were used to identify and measure any defects that occurred during the laser cutting of the electrodes.

IV. ANALYSIS OF THE BURST PROFILES ON THE LASER CUTTING PERFORMANCE

A. Investigated burst profiles

Two different burst shapes were characterized, representing different energy distributions within the bursts, namely, equal pulse (EP) and increasing pulse (IP). Figure 4 shows the two burst shapes for different numbers of pulses in a burst at 31 W average power. The power level was set at this level to allow the EP and IP bursts to be tuned at different pulse repetition rate levels. An increase in the number of pulses within each burst results in a proportional decrease in peak power as shown in Fig. 4. While the photodiode measurements cannot be used to calculate the peak power, the oscilloscope traces can be used to analyze the difference in terms of the peak heights measured in mV. For example, the ratio of the first peak to the second pulse peak for the $Nb = 2$ in the IP profile is approximately 2. By changing the burst shape, the peak power will conform to either an EP or an IP pattern.

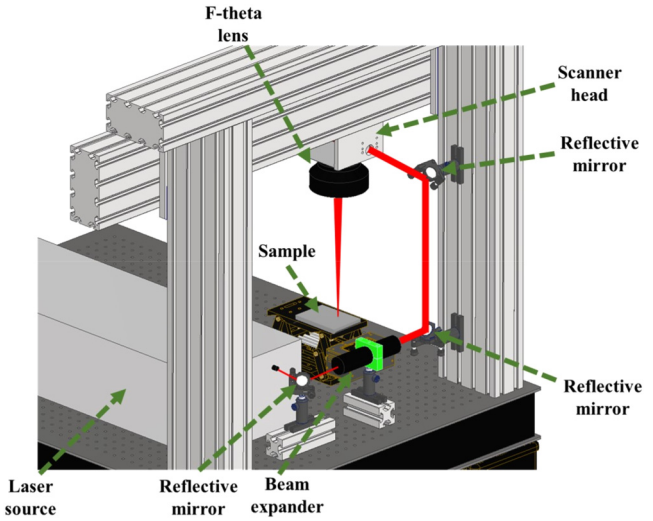

FIG. 3. 3D model of the experimental setup showing the optical path and the processing zone.

B. Experimental design

The experimental investigation was carried out to determine the processability range as a function of burst profile characteristics. The maximum cutting speed was sought by increasing the cutting speed in 0.1 m/s increments at a fixed power level of 31 W. Up to eight pulses within burst counts were examined. Three levels of pulse repetition rate at 200.0, 550.3, and 901.0 kHz were used for the EP shape. Conversely, two frequency levels at 550.3 and 901.0 kHz were tested for the IP shape to see the difference in burst profiles at the higher PRR.

The selection of pulse distribution within the burst was made to explore a novel burst profile shape that had not been studied before. Comparing the profiles of EP and IP bursts helps to understand how to design the burst profile for laser cutting LIB electrodes. All different materials—anode, cathode, Al foil, and Cu foil—were investigated during the experimental campaign to establish representative conditions for notching and cutting. For all experiments, the focal point is positioned on the surface of the sample. Table II shows the fixed and varied parameters used to investigate the laser cutting of electrodes.

The processing conditions were analyzed categorically as "No Cut" and "Cut" conditions. Complete and continuous cut kerfs were sought for a combination of parameters to be classified as "Cut." The conditions that produced the maximum cutting speed were further analyzed to measure burr and kerf width on the bare metals, and kerf width and clearance on the coated materials. Figures 5(a) and 5(b) illustrate example conditions for samples classified as "No Cut" and "Cut." Figure 5(a) shows the burr (w_d) and kerf width measurements on the bare metal collectors, while Fig. 5(c) shows the clearance (w_c) on the electrodes. This figure is just an indicative image to show how the quality parameters were measured for the cathode and anode. For each SEM image, quality indicators were measured at six points from different parts of the image.

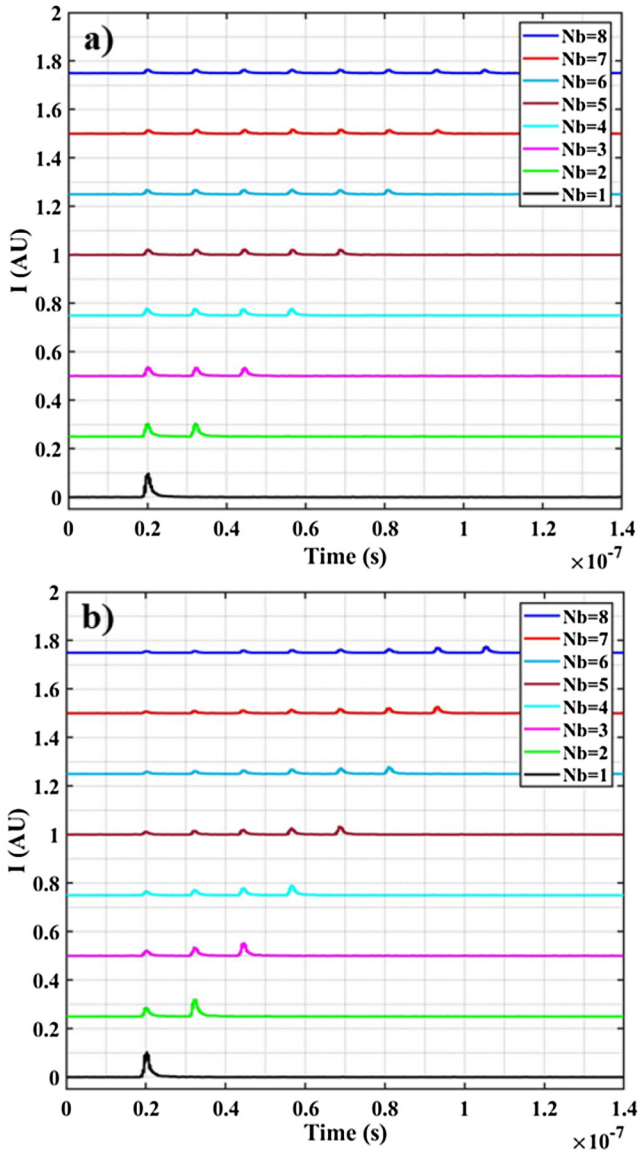

FIG. 4. (a) EP and (b) IP burst shapes for the different number of pulses within a single burst acquired with the fast photodiode at 31 W average power.

After determining the maximum cutting speeds available for each parameter condition, the results were analyzed as a function of the peak power over thickness and peak fluence to assess the driving factors that improve the process productivity in the burst mode.

V. RESULTS

A. Influence of the temporal burst profile on the cutting productivity

Figure 6 shows a comparative analysis of the variation of the maximum cutting speed versus the number of pulses for the cathode, Al foil, anode, and Cu foil with the EP and IP burst shapes. Regarding the cutting speed of the metal foil, it can be seen that increasing *Nb* leads to a significant increase in cutting speed for the EP shape. The productivity of Al foil cutting under the condition of eight pulses is 10.5 times higher than that of a single pulse at 901.0 kHz. The maximum cutting speed for Cu foil is about 2 m/s at 550.3 and 901.0 kHz, and $Nb = 8$. For Cu foil, the maximum cutting speed with eight pulses within the burst is 3.17 times higher than that of a single pulse at 901.0 kHz. For bare metals, the use of high pulse repetition rates and a high number of pulses in the burst seems to be advantageous. The maximum cutting speed for the cathode is 0.7 m/s at 901.0 kHz and $Nb = 8$, while the maximum cutting speed for the anode is 0.4 m/s at 550.3 kHz and $Nb = 8$.

TABLE II. Fixed and variable factors of the experimental campaign.

Fixed factors	
Average power, P_{avg} (W)	31
Focal point, Δz (mm)	0
Variable factors	
Number of pulses, *Nb*	1–2–3–4–5–6–7–8
Pulse repetition rate, PRR (kHz)	200.0–550.3–901.0
Burst shape, BS	Equal peak (EP) – increasing peak (IP)
Material	Anode – cathode – Al foil – Cu foil

The total thickness of the cathode is about six times that of the Al foil. Conversely, the cutting speed of the Al foil is two times higher than that of the cathode without the burst mode condition. However, when the burst mode is used, the cutting speed of the Al foil is about seven times higher than that of the cathode. This illustrates that cutting metallic material with the burst mode is more efficient than cutting coated material. A similar trend is observed for the cathode and the Al foil. This observation can be explained by considering the difference in composition between the coating and the metallic component. From Fig. 6, it can be seen that the transition from the EP to the IP burst shape results in a decrease in the maximum cutting speed for Al and Cu foil from 4.7 and 2.1 m/s to 4.1 and 1.7 m/s, respectively. This reduction is due to the challenge of optimizing the peak fluence for material removal when changing the burst distribution from EP to IP. With the implementation of IP, some peak fluence of initial pulses within the burst may fall below the spallation region. Conversely, there is no change in the maximum cutting speed for the cathode and anode when the burst shape is changed from EP to IP burst shape. This consistency can be explained by the material removal mechanism of the active material, where the temporal distribution of the burst does not affect the interaction between the ultrashort pulses and the active material.

Figures 7 and 8 show SEM images of samples with the highest cutting speed achieved using the EP and IP burst shapes for various combinations of pulse repetition rate, number of pulses, and material type, with the maximum cutting speed indicated in the bottom right corner of each image. Figure 7 shows that increasing the number of pulses within the burst results in a reduction in

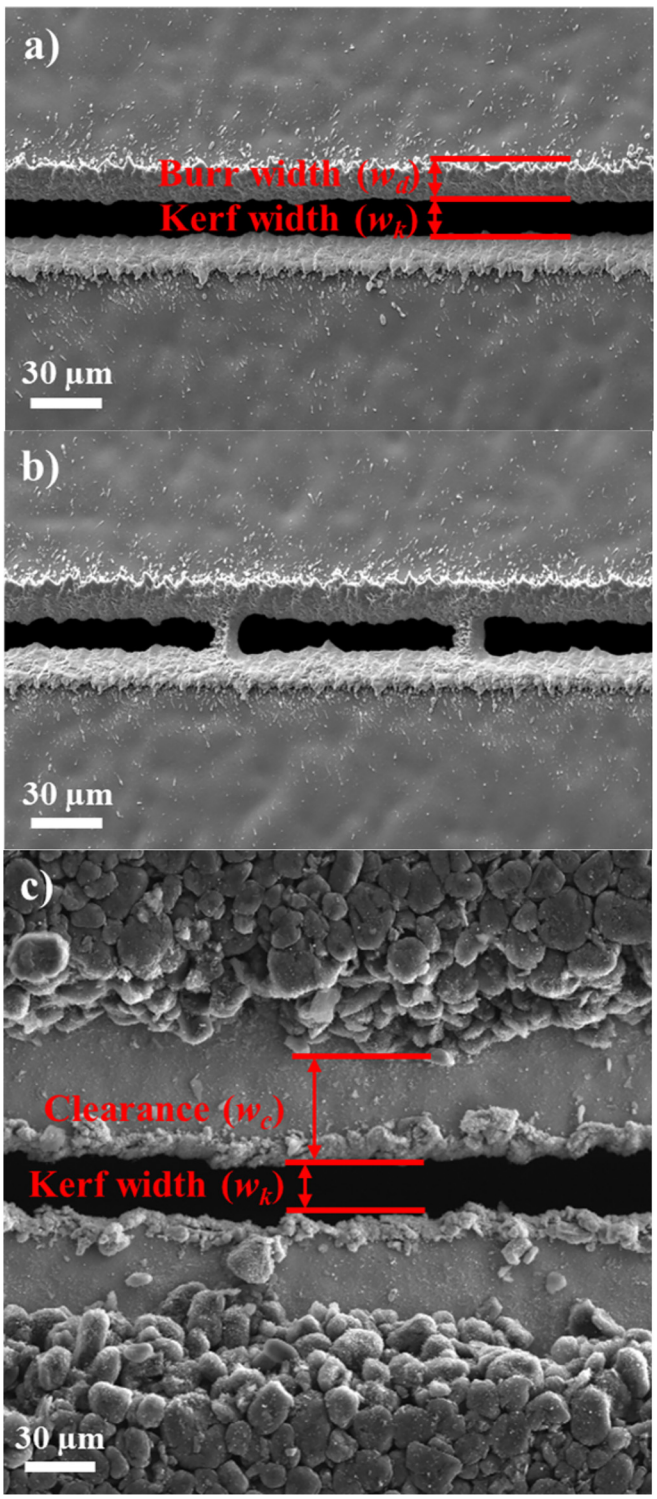

FIG. 5. SEM images of (a) cut sample of Cu foil, (b) partially cut sample of Cu foil, and (c) cut sample of anode with the quality indicators.

anode and cathode clearance. Similarly, it can be seen that increasing the pulse repetition rate results in a reduction in the kerf width. By carefully examining the morphology of the cutting edge of Al and Cu foils for different numbers of pulses, a significant difference can be observed between the cutting edges of samples cut with burst mode and single pulses can be observed. The cutting edge of samples cut with the single pulse appears clean, whereas a resolidified layer of material is present in samples cut with burst mode. Figure 8 shows similar trends across the parameter ranges for the IP burst shape. On the other hand, it is observed that the kerf widths are smaller than those observed for the EP shape.

B. Influence of the temporal burst profile on the cutting quality

Figure 9 illustrates the variation of kerf width versus pulse peak power for all material combinations (Al foil, cathode, Cu foil, and anode) and burst shapes (EP and IP). As shown in Fig. 9, a decrease in the peak fluence results in a decrease in the kerf width. By comparing the kerf width of the samples cut with the EP burst shape, it is clear that using the burst mode for the cathode and anode reduces the kerf width more than the metal foil. In other words, the burst mode is more effective in reducing the kerf width for the cathode and anode than the metal foil.

Figure 10 shows the measured clearance for the cutting of the cathode and anode with EP and IP burst shapes. When the laser irradiates the surface of the active material, it vaporizes the binder, resulting in the ejection of particles.[41] When the laser pulses reach the Cu foil, a shock wave is generated as a result of the ultrashort pulsed laser-material interaction.[42] This interaction initiates the removal of particles from the top and bottom of the electrodes. The shock wave applied to the metal foil causes a reaction force in the active material particles. These particles are bound together with the binder, removing small portions of the active material, resulting in the removal of a larger portion. These phenomena contribute to the formation of clearance on the anode and cathode. This explanation can justify the reduction of the clearance with an increase in the number of pulses. In other words, the interaction between the laser and the metal foil creates an explosive pressure that blows away the active material. In addition, increasing the cutting speed should further reduce the clearance because the active material is exposed to pressure for a relatively shorter time, resulting in the removal of a small portion of the active material.

All factors related to particle cohesion, such as binder type, calendar pressure, and particle size, can affect not only cutting productivity but also clearance. As laser cutting gains more attention in industrial applications, there is a need to investigate the effects of these factors on the laser cutting performance of LIB electrodes.

The burr widths measured from the SEM images are plotted in Fig. 11. The clean edge observed at the cutting edge of samples cut with a single pulse can be attributed to the high pressure exerted on the cutting region, which pushes the molten material downwards during remote laser cutting. However, when the burst mode is used, the pressure on the sample surface is reduced, allowing the molten material to be ejected from the above. Due to the pulse repetition rate, the molten material has sufficient time to resolidify at the edge of the sample.

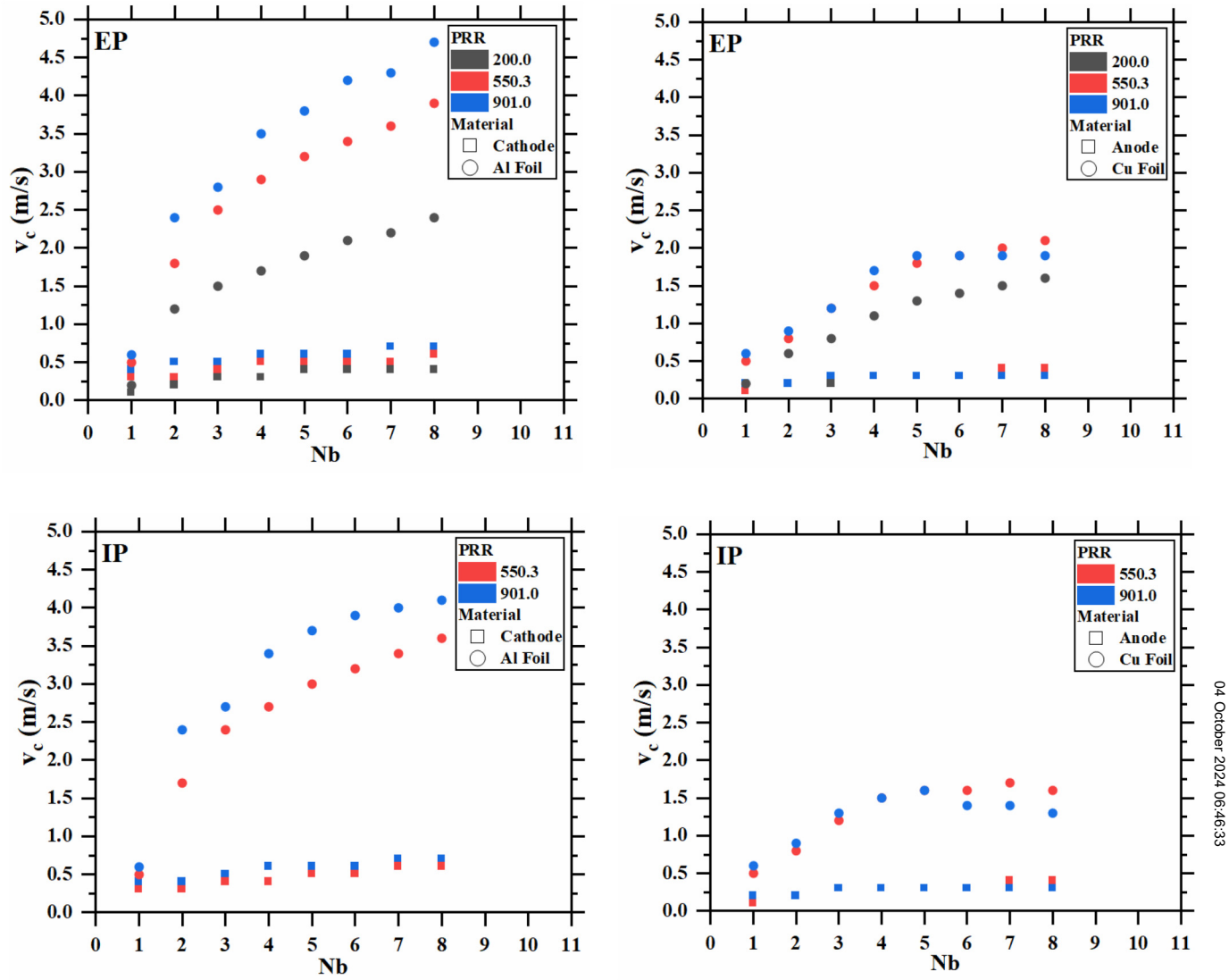

FIG. 6. Maximum cutting speed of Al foil, cathode, Cu foil, and anode vs *Nb* with EP and IP burst shapes with fixed average power at 31 W.

According to Haung *et al.*,[35] the length of Cu foil oxidation was found to be equal to the burr width. This suggests that the burr width is a reliable measure of HAZ for Cu foil. In the case of Al, this phenomenon was even more pronounced due to the higher fluidity and lower surface tension of Al in the melt.[43,44] As a result, the molten material ejected from Al foil has a greater burr width than that of Cu foil.

C. Analysis of cutting efficiency

To better understand the effect of burst shape on laser cutting, the maximum cutting speed is plotted against the peak power over the thickness of each sample. It is important to note that the average energy of the pulses within the burst was used to calculate the peak power for the pulses in the IP. Figures 12(a) and 13(a) illustrate the maximum cutting speed versus the ratio of peak power to material thickness using different burst shapes. It can be seen that for Al foil and cathode a reduction in peak power appears to provide a higher cutting speed. Implementing the EP burst shape allows for faster cutting than IP for Al foil, while the maximum cutting speed of the cathode remains the same for both EP and IP. This suggests that further reduction in peak power could increase the cutting speed for all combinations of EP, IP, Al foil, and cathode. Conversely, Al foil and cathode can achieve faster cutting at lower peak power when EP is used as the burst shape. Comparing the peak power required to cut Al foil and cathode with

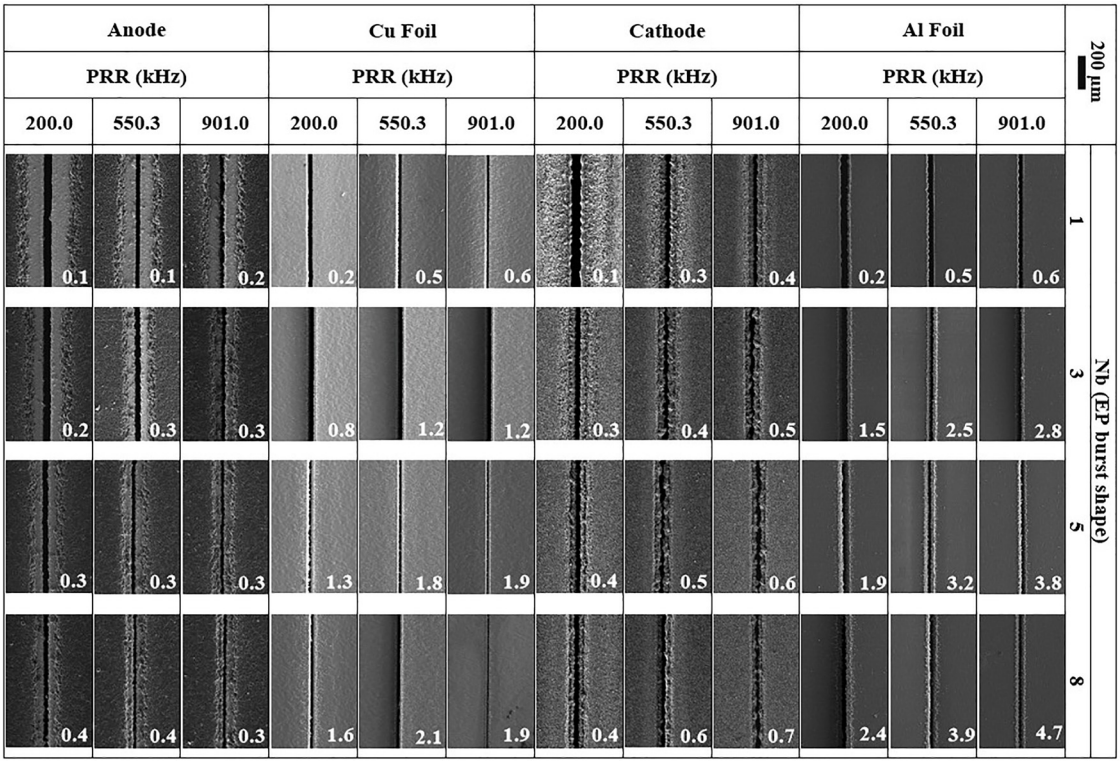

FIG. 7. SEM images of the maximum cutting speed of Al foil, cathode, Cu foil, and anode with the EP burst shape for the combination of pulse repetition rate, and number of pulses in the burst (*Nb* = 1, 3, 5, and 8) with fixed average power at 31 W.

EP, it can be concluded that the cathode requires less peak power than Al foil. According to Fig. 12(a), the peak power normalized by thickness for Al foil and cathode cut with EP is lower than that cut with IP. This indicates that EP can achieve cutting with lower average power. In other words, using the IP burst shape to cut cathode and Al foil results in wasted laser energy. As shown in Fig. 13(a), for Cu foil and anode, the maximum cutting speed is achieved at an intermediate peak power and decreases as the peak power increases. There is no clear distinction between the burst shapes for anode cutting. However, for Cu foil cutting, the use of the EP burst shape allows cutting at a higher speed than the IP shape. There appears to be an optimum level of peak power (peak fluence) for Cu foil laser cutting. This is because reducing the pulse energy increases the cutting speed up to a certain threshold, beyond which the cutting speed decreases. The observed condition does not follow the expected trend of increasing cutting speed. Rather than maintaining the same cutting speed at the same average power or increasing the cutting speed at a higher peak power, the results suggest that it is beneficial to reduce the peak power in order to cut faster at the same average power with a higher repetition rate.

Figures 12(b) and 13(b) show the volume of material removed per pulse energy plotted against the peak fluence. For a given material, the expected shape of the data distribution should follow a rapidly increasing initial removed material volume per pulse energy starting from the ablation threshold to a maximum and a slow decay with the increasing peak fluence according to the form of Eq. (6). Figure 12(b) shows that for both Al foil and cathode the ablation efficiency in terms of volume removed per energy decreases as the peak fluence level increases. The lack of a clear peak indicates a possible reduction in peak fluence may have resulted in an increase in ablation efficiency. The ablation efficiency appears to be similar for the cathode and the Al foil as the results overlap. Figure 13(b) shows a peak in the ablation efficiency for both the anode and the Cu foil at around 6 J/cm^2 for the anode and 5 J/cm^2 for the Cu foil. The graph also shows that the overall ablation efficiency is higher for the anode compared to the Cu foil.

Figure 14 shows the estimated values for the ablation threshold fluence and penetration depth of a single pulse for different combinations of materials (Al foil, cathode, Cu foil, and anode) and burst shapes (IP and EP) using Eq. (6). In other words, the ablation threshold fluence and penetration depth are estimated by fitting the data from Figs. 12(b) and 13(b) into Eq. (6). It can be seen that the threshold fluence of Cu foil and anode is relatively higher than that of Al foil and cathode.

VI. DISCUSSION

The results provide insight into the benefits of using burst mode when cutting electrode materials. It is evident that the splitting of a

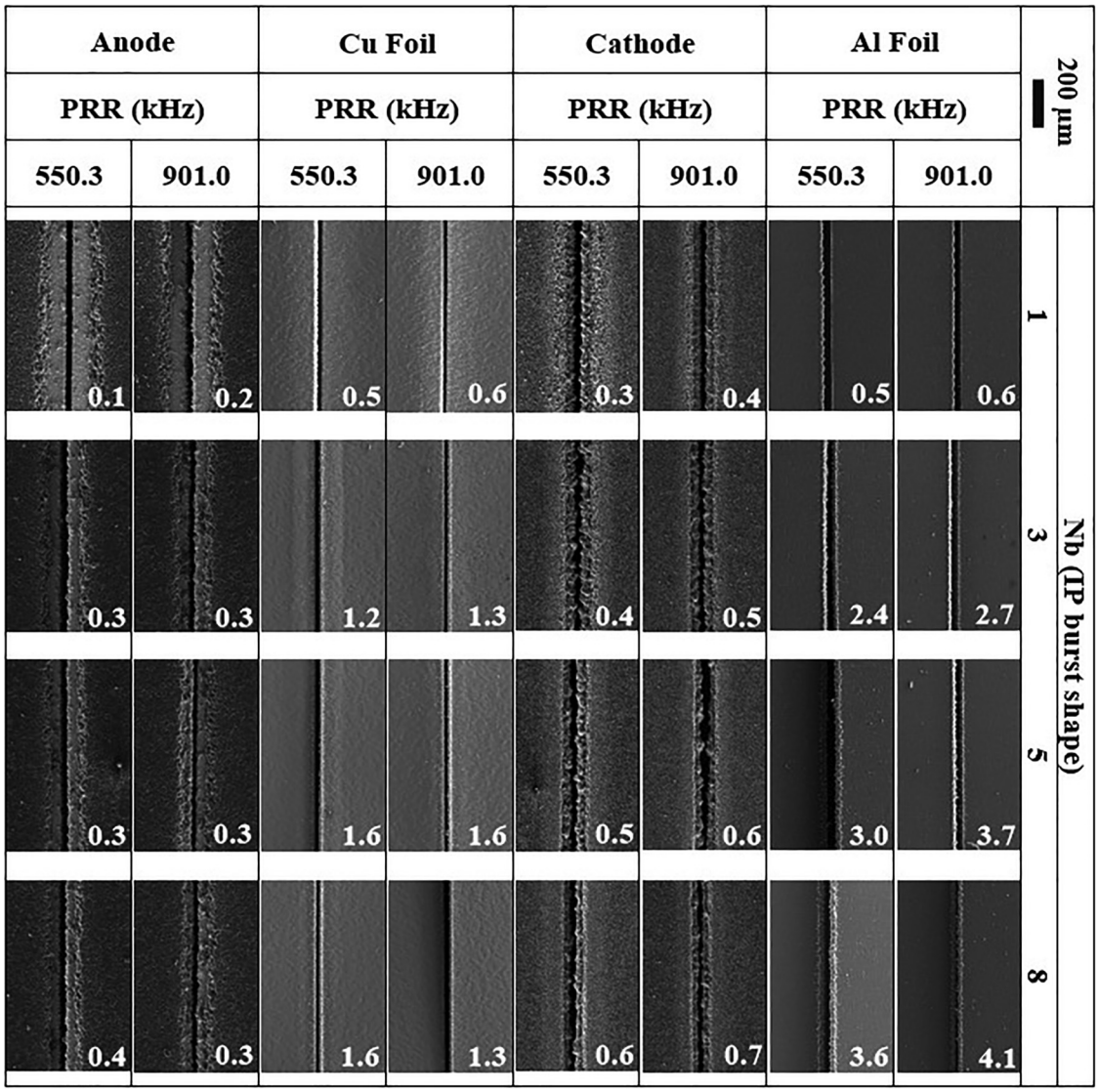

FIG. 8. SEM images of the maximum cutting speed of Al foil, cathode, Cu foil, and anode with the IP burst shape for the combination of pulse repetition rate, and number of pulses in the burst (*Nb* = 1, 3, 5, and 8) with fixed average power at 31 W.

single high energy pulse into smaller burst trains improves productivity. From this perspective, the results suggest that the high peak power essentially produces a wider kerf rather than a deeper cut depth. If the focal point remains fixed on top of the sample, this reduction in peak power results in a reduction in peak fluence. According to the two-temperature model, when the peak fluence exceeds the optimum value for material removal, the effective penetration depth of the energy decreases, and much of the energy diffuses laterally.[45] The model based on the ratio of peak power to thickness ratio [Eq. (4)] does not provide a clear explanation of cutting speed. In fact, the cutting speed is slower at higher peak powers.

On the other hand, the relationship between the peak fluence and the volume per energy removed was confirmed. The results showed that for Al foil and cathode, a further reduction in pulse energy may be required, while for Cu foil and anode, the peak points could be individualized. These results were obtained by calculating the energy of the single pulses within the burst packages, neglecting any possible effect of the pulse repetition rate. The use of EP power profiles resulted in higher overall cutting speeds. The IP profile reduced the cutting speeds. This observation implies that the energy in separate pulses within the burst interacts with the material in an independent manner for the given beam/material

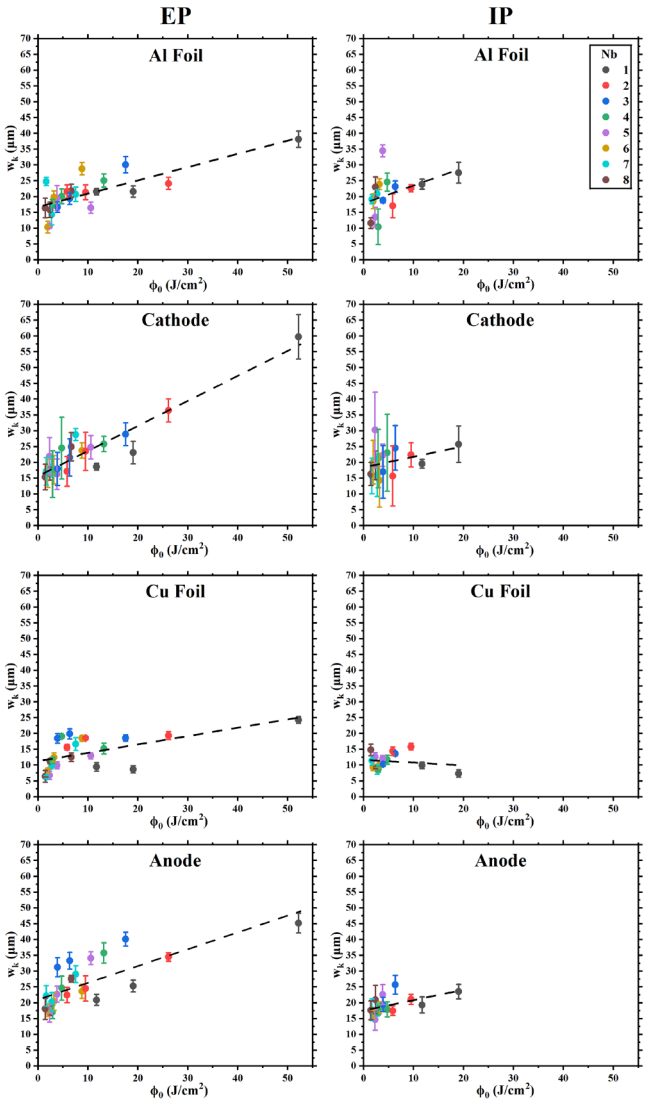

FIG. 9. Kerf width variation vs peak fluence for the maximum cutting speed of Al foil, cathode, Cu foil, and anode with the EP and IP burst shapes with fixed average power at 31 W. Dashed lines depict trend only.

combination. It is observed that the initial pulses in a burst do not significantly affect the interaction of the subsequent pulses. Accordingly, as a first approximation, it can be stated that the advantage of the burst mode is to increase the pulse repetition rate at lower pulse energy, rather than to change the interaction mechanisms between successive pulses in the burst when processing electrode materials. This allows the optimum peak fluence strategy to be sought for both composite electrode materials and pure metal foils. The differences between the materials in terms of the ablation efficiency can be attributed to the compactness of the coating layers, the binder

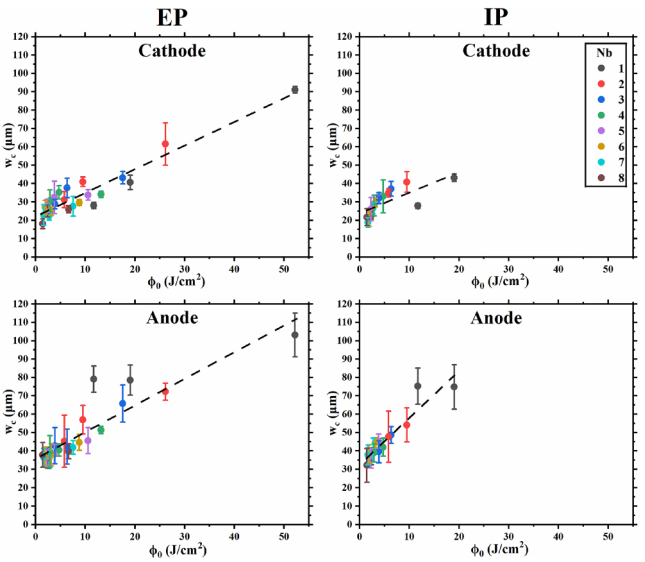

FIG. 10. Clearance variation vs peak fluence for the maximum cutting speed of cathode and anode with EP and IP burst shapes with fixed average power at 31 W. Dashed lines depict trend only.

content, and the type of binder used, all of which contribute to the material removal mechanism.

In order to find the optimum peak fluence to improve the productivity of the laser cutting of electrodes, the different

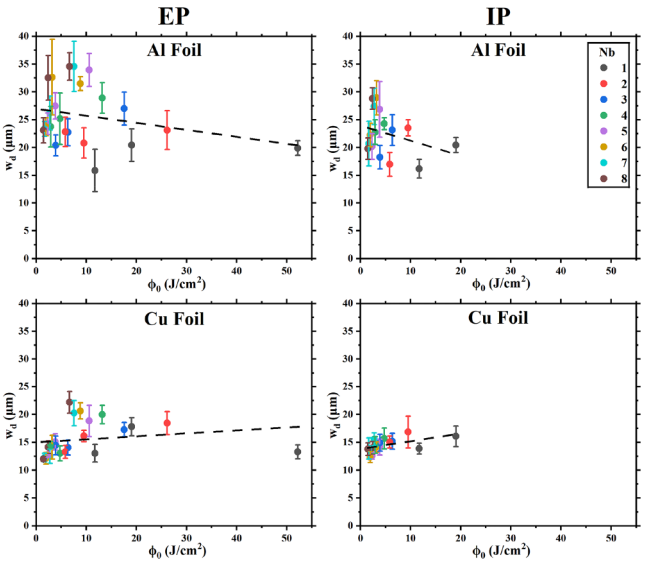

FIG. 11. Burr width against peak fluence for the maximum cutting speed of Al and Cu foil with EP and IP burst shapes with fixed average power at 31 W. Dashed lines depict trend only.

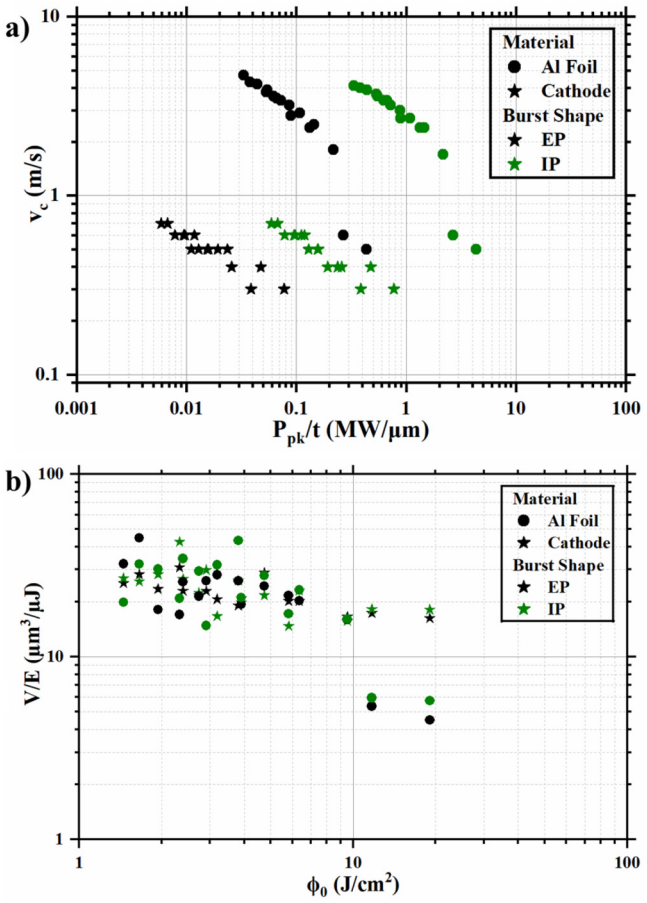

FIG. 12. (a) Maximum cutting speed vs peak power to material thickness ratio and (b) energy specific volume against peak fluence for Al foil and cathode with EP and IP burst shape with fixed average power at 31 W.

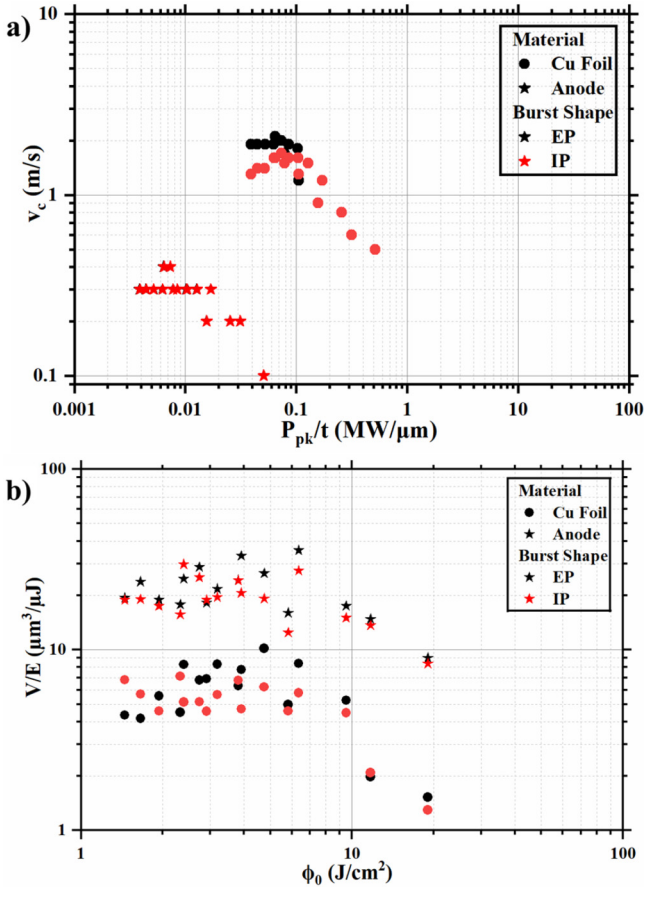

FIG. 13. (a) Maximum cutting speed vs peak power to material thickness ratio and (b) energy specific volume against peak fluence for Cu foil and anode with EP and IP burst shape with fixed average power at 31 W.

interactions between the ultrashort laser and the metal can be analyzed in detail. Typically, three separate regions are considered in relation to the ablation threshold fluence, as follows:

- Melting of the metal surface ($\phi_0 < \phi_{th}$),
- Spallation of the metal surface ($\phi_{th} < \phi_0 < \phi_{0,\mathrm{opt}}$),
- Phase explosion ($\phi_0 \gg \phi_{0,\mathrm{opt}}$).

As the peak fluence increases, heating and subsequent melting begin. This increase in peak fluence induces pressure generation within the interaction zone. When the peak fluence is about $e^2 = 7.4$ times the ablation threshold fluence, the material removal per pulse energy peaks. Further increase in peak fluence leads to the formation of particles and clusters in a gaseous state which begin to ionize. This ionized gaseous state results in a shielding effect, which subsequently reduces the material removal per pulse energy. The ablation threshold for Cu with ps-pulsed lasers in the near-infrared wavelength is known to be higher than that for Al.[46–48] This confirms the need for further peak fluence reduction for Al foil and cathode compared to Cu foil and anode. In order to optimize the parameters of the ultrashort pulse laser process, it is imperative to adjust them toward the optimum value.[49]

With the advent of high-power ultrashort laser systems, the pulse energy typically exceeds the optimized value. Increasing the spot diameter and using burst mode are potential options to reduce the peak fluence. However, increasing the spot diameter may not be an effective method for cutting metal foil because it primarily increases the molten area, which is undesirable. Conversely, increasing the number of pulses within the burst and adjusting the pulse repetition rate will reduce the pulse energy. In other words, maintaining the focal point on the sample surface while increasing the number of pulses within the burst and adjusting the pulse repetition rate will facilitate a reduction in the peak power of the pulse. Using the calculated threshold fluences in the EP burst shape for Al and Cu foils, it is possible to derive results for ideal laser source characteristics. Using the estimated threshold fluence and the

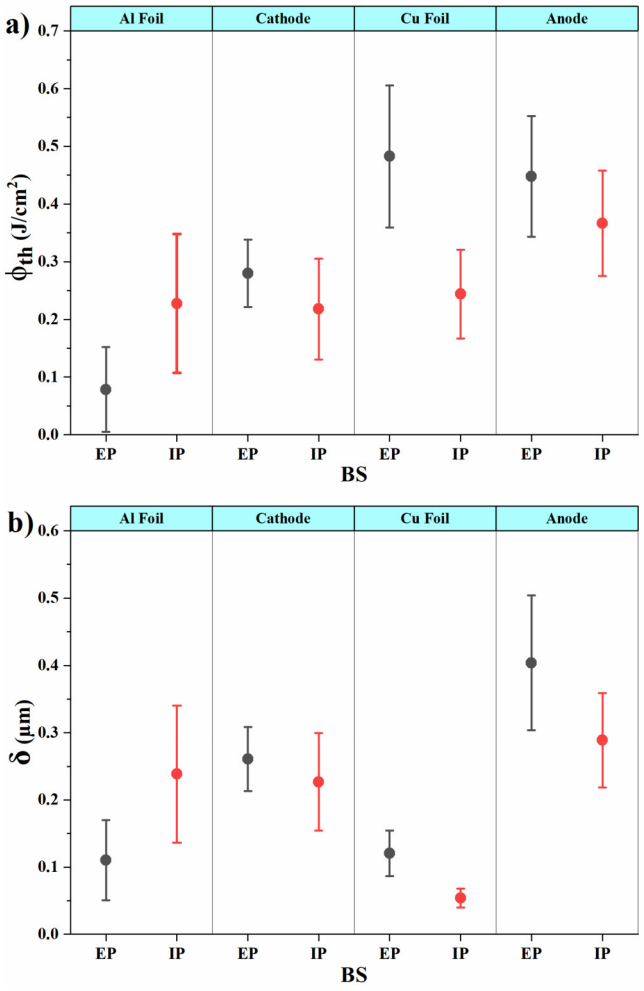

FIG. 14. Estimated (a) ablation threshold and (b) penetration depth of single pulse for the Al foil, cathode, Cu foil, and anode with EP and IP burst shape using Eq. (6). Error bars represent 95% confidence interval for the mean.

effective penetration depth, it is possible to calculate the optimum peak fluence, pulse energy, pulse repetition rate, and average power required to cut the Al foil and Cu foils for a given productivity requirement expressed in terms of cutting speed. Since Eq. (9) depends on the kerf width, the kerf width is considered the diameter of the beam at the focal point as predicted by the analytical model ($d_0 = 27.5\,\mu$m). The specifications of the ideal ultrashort pulse laser system for cutting Al and Cu foils are shown in Table III for medium and high productivity solutions corresponding to 1 and 5 m/s, respectively. It should be noted that the calculation to derive the required pulse repetition rate is based on single pulses.

In order for this laser system to cut Al and Cu foils at a cutting speed comparable to mechanical cutting (1 m/s), the average power of the laser system should be 9.5 and 45 W at the pulse repetition rates of 5.5 and 4.2 MHz, respectively. The predictions are in agreement with the experimental results. On the other hand, the predictions for 5 m/s indicate the need to increase the pulse repetition rate to 27.28 and 21.14 MHz for Al and Cu foils, respectively. The corresponding average power levels are predicted to be 47 and 224.2 W, respectively. The scalability of the cutting speed by increasing the pulse repetition rate requires an experimental validation. Similar estimates for anode and cathode materials are more difficult to make due to the layered structure. However, in this case, the increase in performance by increasing the pulse repetition rate seems to be more advantageous. The active material on the anode and cathode materials consists of particles bound together with a binder. Schmieder[41] investigated the energy required to ablate the active material, providing practical insights into its removal. A significant discrepancy was found between these energy values. Subsequently, it was shown that the mechanism of laser removal of the active material involves the ablation of the binder, which has a lower evaporation temperature, followed by the ejection of the particles. It was observed that the evacuation time was relatively longer than the pulse duration of the ns-pulsed laser source. Although there is a lack of scientific literature on the interaction between ultrashort lasers and active material, the results of Schmieder[41] suggest a different mechanism for material removal in the case of active material. This difference may explain the lower efficiency observed when using the burst mode to cut the cathode and anode. While the ablation threshold of a composite material such as the anode and the cathode is difficult to determine with a single value, the approach shown in this work may be an effective way of providing the apparent optimum peak fluence values.

VII. CONCLUSIONS

Laser cutting of Al foil, cathode, Cu foil, and anode was investigated by varying the number of pulses per burst (from 1 to 8), pulse repetition rate (200.0, 550.3, and 901.0 kHz), and burst shape (EP and IP) while keeping the average power fixed.

Increasing the number of pulses in the burst and increasing the pulse repetition rate help to reduce the peak fluence of each

TABLE III. Specifications of ideal laser sources to cut the Al and Cu foil at 1 and 5 m/s cutting speeds with a focused beam size of $d_0 = 27.5\,\mu$m.

Material	v_c (m/s)	δ (μm)	ϕ_{th} (J/cm^2)	$\phi_{0,opt}$ (J/cm^2)	PRR (MHz)	E (μJ)	P_{avg} (W)
Al foil	1	0.11	0.08	0.58	5.46	1.72	9.4
Cu foil	1	0.12	0.48	3.57	4.23	10.60	44.8
Al foil	5	0.11	0.08	0.58	27.28	1.72	47.0
Cu foil	5	0.12	0.48	3.57	21.14	10.60	224.2

pulse, making it easier to use the optimum peak fluence for cutting metal foil. For instance, using the burst mode under optimum conditions can increase the cutting speed from 0.6 to 4.7 m/s for Al foil and from 0.5 to 2.1 m/s for Cu foil, achieving the highest cutting speeds for these metal foils. The effect of the burst mode on the cutting speed of the anode and cathode is less significant but still noticeable. For instance, in the best case, the cutting speed of the anode and cathode can be increased from 0.1 to 0.4 m/s and from 0.4 to 0.7 m/s, respectively, by increasing the number of pulses in the burst from 1 to 8. The analysis showed that there is an optimum peak fluence for each type of material during ps-pulsed cutting operations. The results confirmed that the burst mode improved the cutting speed by reducing the pulse energy toward the ideal pulse energy at the same power level, thereby driving the process toward the optimum peak fluence values. While the optimum peak fluence value for cutting Cu foil appears to have been found experimentally, further reductions in the pulse energy were found to be possible for cutting the Al foil. Scaling up of the process by estimating the ideal pulse energy and increasing the pulse repetition rate appears to be a viable option. For the composite anode and cathode materials, direct calculations of energy and pulse repetition rates are more difficult to establish, although the presence of an optimum peak fluence level could be observed. This highlights the different mechanisms of laser-metallic material interaction and laser-active material interaction in LIB electrode cutting. Nevertheless, further research is needed to understand the laser-active material interaction in detail, as there is a lack of publications on this topic for the ultrashort laser system. In terms of quality, it was observed that reducing the peak fluence of the pulse leads to an increase in the quality of the cut for all parameter and material combinations. The results of this work highlight that the next generation of high-power ultrashort pulse lasers for electrode cutting would benefit from moderate energy levels and pulse repetition rates in the MHz range.

ACKNOWLEDGMENTS

The authors are grateful to Comau for the support provided for the research project of PHO. This project has been partially funded within the National Recovery and Resilience (PNRR) fund under Scholarship No. 38-033-16-DOT1316301-3558. Lumentum is gratefully acknowledged for the technical support provided to the work.

AUTHOR DECLARATIONS

Conflict of Interest

The authors have no conflicts to disclose.

Author Contributions

Pourya Heidari Orojloo: Conceptualization (equal); Data curation (equal); Formal analysis (equal); Investigation (equal); Methodology (equal); Software (equal); Validation (equal); Visualization (equal); Writing – original draft (equal); Writing – review & editing (equal). **Ali Gökhan Demir:** Conceptualization (equal); Data curation (equal); Formal analysis (equal); Funding acquisition (equal); Investigation (equal); Methodology (equal); Resources (equal); Software (equal); Supervision (equal); Validation (equal); Visualization (equal); Writing – original draft (equal); Writing – review & editing (equal).

REFERENCES

[1]A. Parikh, M. Shah, and M. Prajapati, "Fuelling the sustainable future: A comparative analysis between battery electrical vehicles (BEV) and fuel cell electrical vehicles (FCEV)," Environ. Sci. Pollut. Res. **30**, 57236–57252 (2023).
[2]J. Fleischmann, M. Hanicke, E. Horetsky, D. Ibrahim, S. Jautelat, M. Linder, P. Schaufuss, L. Torscht, and A. van de Rijt, *Battery 2030: Resilient, Sustainable, and Circular* (McKinsey & Company, 2023), pp. 2–18.
[3]Y. Liu, R. Zhang, J. Wang, and Y. Wang, "Current and future lithium-ion battery manufacturing," iScience **24**, 102332 (2021).
[4]Sebastian Wolf, Niklas Schwenzer, Tim Tratz, Vinzenz Göken, Markus Börner, Daniel Neb, Heiner Heimes, Martin Winter, and Achim Kampker, "Optimized $LiFePO_4$-based cathode production for lithium-ion batteries through laser- and convection-based hybrid drying process," World Electr. Veh. J. **14**, 281–291 (2023).
[5]A. Ascari, C. Angeloni, E. Liverani, and A. Fortunato, "High speed laser cutting of ultrathin metal foils for battery cell production," J. Laser Appl. **35**, 042063 (2023).
[6]R. Baumann, S. Alamri, A. I. Aguilar-Morales, A. F. Lasagni, and T. Kunze, "Advanced remote laser cutting of battery foils using an interference approach," Mater. Lett. X **14**, 100138 (2022).
[7]D. Lee, "Investigation of physical phenomena and cutting efficiency for laser cutting on anode for Li-Ion batteries," Appl. Sci. (Switzerland) **8**, 266–280 (2018).
[8]M. R. Kronthaler, F. Schloegl, J. Kurfer, R. Wiedenmann, M. F. Zaeh, and G. Reinhart, "Laser cutting in the production of lithium ion cells," Phys. Procedia **39**, 213–224 (2012).
[9]Matthias Luetke, Volker Franke, Anja Techel, Thomas Himmer, Udo Klotzbach, Andreas Wetzig, and Eckhard Beyer, "A comparative study on cutting electrodes for batteries with lasers," Phys. Procedia **12**, 286–291 (2011).
[10]M. G. Berhe, H. G. Oh, S. K. Park, and D. Lee, "Laser cutting of silicon anode for lithium-ion batteries," J. Mater. Res. Technol. **16**, 322–334 (2022).
[11]T. Reincke, S. Kreling, and K. Dilger. "The influences of pulse overlap on cut quality during fiber laser cutting of electrodes for lithium-ion batteries," in *Proceedings of the Lasers in Manufacturing Conference*, Berlin, Germany, 2015, pp. 22–25.
[12]L. N. Trinh and D. Lee, "The characteristics of laser welding of a thin aluminum tab and steel battery case for lithium-ion battery," Metals (Basel) **10**, 1–15 (2020).
[13]A. Olowinsky, C. Spurk, J. Helm, and A. Gillner, "Laser-based joining of electrode stacks for automated large-scale production of Li-ion battery cells," Energy Technol. **11**, 2200770 (2023).
[14]L. N. Trinh and D. Lee, "Welding of thin tab and battery case for lithium-ion battery cylindrical cell using nanosecond pulsed fiber laser," J. Weld. Join. **38**, 389–394 (2020).
[15]S. Grabmann, J. Kriegler, F. Harst, F. J. Günter, and M. F. Zaeh, "Laser welding of current collector foil stacks in battery production–mechanical properties of joints welded with a green high-power disk laser," Int. J. Adv. Manuf. Technol. **118**, 2571–2586 (2022).
[16]W. Pfleging and P. Gotcu, "Femtosecond laser processing of thick film cathodes and its impact on lithium-ion diffusion kinetics," Appl. Sci. (Switzerland) **9**, 3588 (2019).
[17]P. Zhu, H. J. Seifert, and W. Pfleging, "The ultrafast laser ablation of Li$(Ni_{0.6}Mn_{0.2}Co_{0.2})O_2$ electrodes with high mass loading," Appl. Sci. (Switzerland) **9**, 4067 (2019).
[18]M. Gebrekiros Berhe, H. G. Oh, S. K. Park, M. Mondal, and D. Lee, "Effect of laser-induced groove morphology on the wettability and performance of lithium-ion batteries," Mater. Des. **231**, 112020 (2023).

[19]S. Ali and J. Shin, "In-depth characterization of laser-welded aluminum-and-copper dissimilar joint for electric vehicle battery connections," Materials **15**, 7463 (2022).
[20]M. Francioso, C. Angeloni, A. Fortunato, E. Liverani, and A. Ascari, "Experimental investigation on the effect of nickel-plating thickness on continuous-wave laser welding of copper and steel Tab joints for battery manufacturing," Lasers Manuf. Mater. Process. **11**, 353–370 (2024).
[21]Z. Liu, K. Wang, H. He, J. Xie, and W. Huang, "Method for evaluating laser welding quality of battery module based on coupling model," J. Power Sources **546**, 231959 (2022).
[22]J. Kriegler, T. M. D. Nguyen, L. Tomcic, L. Hille, S. Grabmann, E. I. Jaimez-Farnham, and M. F. Zaeh, "Processing of lithium metal for the production of post-lithium-ion batteries using a pulsed nanosecond fiber laser," Res. Mater. **15**, 100305 (2022).
[23]T. Jansen, D. Blass, S. Hartwig, and K. Dilger, "Processing of advanced battery materials – laser cutting of pure lithium metal foils," Batteries **4**, 37–52 (2018).
[24]J. Kriegler, E. Jaimez-Farnham, L. Hille, E. Dashjav, and M. F. Zaeh, "Pulsed laser ablation of a ceramic electrolyte for all-solid-state batteries," Procedia CIRP **111**, 800–805 (2022).
[25]T. Jansen, S. Hartwig, D. Blass, and K. Dilger, "Laser cutting of pure lithium metal anodes—Effects of atmospheric conditions," Laser Inst. Am. **2017**, 602–610 (2017).
[26]A. G. Demir and B. Previtali, "Remote cutting of Li-ion battery electrodes with infrared and green ns-pulsed fibre lasers," Int. J. Adv. Manuf. Technol. **75**, 1557–1568 (2014).
[27]A. H. A. Lutey, M. Fiorini, A. Fortunato, and S. Carmignato, "Lithium iron phosphate battery electrode integrity following high speed pulsed laser cutting," Appl. Phys. A **119**, 431–435 (2015).
[28]D. Lee and S. Ahn, "Investigation of laser cutting width of $LiCoO_2$ coated aluminum for lithium-ion batteries," Appl. Sci. (Switzerland) **7**, 914–925 (2017).
[29]J. Kriegler, M. Binzer, and M. F. Zaeh, "Process strategies for laser cutting of electrodes in lithium-ion battery production," J. Laser Appl. **33**, 012006 (2021).
[30]D. Lee, R. Patwa, H. Herfurth, and J. Mazumder, "High speed remote laser cutting of electrodes for lithium-ion batteries: Anode," J. Power Sources **240**, 368–380 (2013).
[31]D. Lee, R. Patwa, H. Herfurth, and J. Mazumder, "Three dimensional simulation of high speed remote laser cutting of cathode for lithium-ion batteries," J. Laser Appl. **28**, 032010 (2016).
[32]D. Lee, R. Patwa, H. Herfurth, and J. Mazumder, "Computational and experimental studies of laser cutting of the current collectors for lithium-ion batteries," J. Power Sources **210**, 327–338 (2012).
[33]P. Mannion, J. Magee, E. Coyne, and G. M. O'connor, see http://spiedl.org/terms for "Ablation thresholds in ultrafast laser micro-machining of common metals in air," 2003.
[34]B. Neuenschwander, T. Kramer, B. Lauer, and B. Jaeggi, "Burst mode with ps-and fs-pulses: Influence on the removal rate, surface quality and heat accumulation," Laser Appl. Microelectron. Optoelectron. Manuf. **9350**, 79–92 (2015).
[35]J. Huang, W. Shi, J. Huang, Y. Xie, Y. Ba, and K. He, "High speed pulsed laser cutting of anode material for a Li-ion battery in burst mode," Opt. Mater. Express **11**, 2300–2309 (2021).
[36]B. N. Chichkov, C. Momma, S. Nolte, F. Von Alvensleben, and A. Tünnermann. "Femtosecond, picosecond and nanosecond laser ablation of solids." Appl. Phys. A **63**, 109–115 (1996).
[37]G. Račiukaitis, M. Brikas, P. Gečys, B. Voisiat, and M. Gedvilas, "Use of high repetition rate and high power lasers in microfabrication: How to keep the efficiency high?," J. Laser Micro Nanoeng. **4**, 186–191 (2009).
[38]B. Neuenschwander, B. Jaeggi, M. Schmid, and G. Hennig, "Surface structuring with ultra-short laser pulses: Basics, limitations and needs for high throughput," Phys. Procedia **56**, 1047–1058 (2014).
[39]B. Neuenschwander, G. F. Bucher, G. Hennig, C. Nussbaum, B. Joss, M. Muralt, S. Zehnder, U. W. Hunziker, and P. Schütz. "Processing of dielectric materials and metals with ps laserpulses," in *Pacific International Conference on Applications of Lasers and Optics* (ASME, 2010), pp. 707–715.
[40]J. Furmanski, A. M. Rubenchik, M. D. Shirk, and B. C. Stuart, "Deterministic processing of alumina with ultrashort laser pulses," J. Appl. Phys. **102**, 073112 (2007).
[41]B. Schmieder, "Analytical model of the laser ablation mechanism of lithium-ion battery coatings," Proc. SPIE **9351**, 296–308 (2015).
[42]Maximilian Spellauge, Jan Winter, Stephan Rapp, Cormac McDonnell, Florian Sotier, Michael Schmidt, and Heinz P. Huber, "Influence of stress confinement, particle shielding and re-deposition on the ultrashort pulse laser ablation of metals revealed by ultrafast time-resolved experiments," Appl. Surf. Sci. **545**, 148930 (2021).
[43]D. A. Harrison, D. Yan, and S. Blairs. "The surface tension of liquid copper," J. Chem. Thermodynam. **9**(12), 1111–1119 (1977).
[44]I. F. Bainbridge and J. A. Taylor, "The surface tension of pure aluminum and aluminum alloys," Metall. Mater. Trans. A **44**, 3901–3909 (2013).
[45]Shijie Song, Qinghua Lu, Peilei Zhang, Hua Yan, Haichuan Shi, Zhishui Yu, Tianzhu Sun, Zhirong Luo, and Yingtao Tian, "A critical review on the simulation of ultra-short pulse laser-metal interactions based on a two-temperature model (TTM)," Opt. Laser Technol. **159**, 109001 (2023).
[46]G. Raciukaitis, M. Brikas, P. Gecys, and M. Gedvilas, "Accumulation effects in laser ablation of metals with high-repetition-rate lasers," Proc. SPIE **7005**, 725–735 (2008).
[47]E. G. Gamaly, N. R. Madsen, M. Duering, A. V. Rode, V. Z. Kolev, and B. Luther-Davies, "Ablation of metals with picosecond laser pulses: Evidence of long-lived nonequilibrium conditions at the surface," Phys. Rev. B **71**, 174405 (2005).
[48]A. Žemaitis, P. Gečys, M. Barkauskas, G. Račiukaitis, and M. Gedvilas, "Highly-efficient laser ablation of copper by bursts of ultrashort tuneable (fs-ps) pulses," Sci. Rep. **9**, 12280 (2019).
[49]D. J. Förster, B. Jäggi, A. Michalowski, and B. Neuenschwander, "Review on experimental and theoretical investigations of ultra-short pulsed laser ablation of metals with burst pulses," Materials **14**, 3331–3370 (2021).